Community effects allow bioelectrical reprogramming of cell membrane potentials in multicellular aggregates: Model simulations

Javier Cervera,[1] Patricio Ramirez,[2] Michael Levin,[3] and Salvador Mafe[1,*]
[1]*Departamento Termodinàmica, Universitat de València, E-46100 Burjassot, Spain*
[2]*Departamento Física Aplicada, Universidad Politécnica de Valencia, E-46022 Valencia, Spain*
[3]*Department of Biology and Allen Discovery Center at Tufts University, Medford, Massachusetts 02155–4243, USA*

(Received 4 August 2020; accepted 4 November 2020; published 25 November 2020)

Bioelectrical patterns are established by spatiotemporal correlations of cell membrane potentials at the multicellular level, being crucial to development, regeneration, and tumorigenesis. We have conducted multicellular simulations on bioelectrical community effects and intercellular coupling in multicellular aggregates. The simulations aim at establishing under which conditions a local heterogeneity consisting of a small patch of cells can be stabilized against a large aggregate of surrounding identical cells which are in a different bioelectrical state. In this way, instructive bioelectrical information can be persistently encoded in spatiotemporal patterns of separated domains with different cell polarization states. The multicellular community effects obtained are regulated both at the single-cell and intercellular levels, and emerge from a delicate balance between the degrees of intercellular coupling in: (i) the small patch, (ii) the surrounding bulk, and (iii) the interface that separates these two regions. The model is experimentally motivated and consists of two generic voltage-gated ion channels that attempt to establish the depolarized and polarized cell states together with coupling conductances whose individual and intercellular different states permit a dynamic multicellular connectivity. The simulations suggest that community effects may allow the reprogramming of single-cell bioelectrical states, in agreement with recent experimental data. A better understanding of the resulting electrical regionalization can assist the electroceutical correction of abnormally depolarized regions initiated in the bulk of normal tissues as well as suggest new biophysical mechanisms for the establishment of target patterns in multicellular engineering.

DOI: 10.1103/PhysRevE.102.052412

I. INTRODUCTION

The emergence of biological patterns results from the interplay of (i) a protein specification encoded in the genome at the single-cell level and (ii) the intercellular signals that orchestrate the whole system at the multicellular level. Patterns are supported on genetically determined hardware but operationally established by the biological signals that allow spatiotemporal correlations among different cells. A distributed electrical control, complementary to the biochemical [1] and biomechanical [2] regulations, is also involved in these multicellular correlations [3–5]. In this control, the cell membrane acts as a central bioelectrical interface between the external microenvironment, including the neighboring cells, and the cell cytoplasm. This interface must regulate the multiscale spatial and temporal requirements of sensing and actuating. Indeed, the partial isolation, limited extension, and relatively large time responses of most cellular organelles could not appropriately resolve the external intercellular signals required for multicellular patterning [3,6–9].

At the single-cell level, the ion channel proteins form the membrane aqueous pores that allow a rapid bioelectrical response to environmental changes. In particular, the cell potential V, which is defined as the electric potential difference between the cell inside and outside, can regulate the entry of signaling cations (e.g., potassium and calcium) and biochemical messengers (e.g., serotonin and butyrate). The specific functions of proteins and membrane lipids are influenced by the ionic concentrations [5,6,10,11]. In turn, V is modulated by these concentrations and the ion channel conductances, thus forming a feedback control system [5,6,10]. At the multicellular scale, the intercellular gap junction proteins connecting adjacent cell membranes permit us to interchange the biophysical information that is needed to establish and operate complex dynamic patterns [5,12–15].

Spatial patterns of electric potential distributions have now been described in a range of model systems, including chick, frog, zebrafish [16,17], and even classical genetic models such as Drosophila [18]. These potential distributions are known to occur as instructive endogenous prepatterns for the morphogenesis of the eye [19], brain [20,21], and face [22,23], as well as pathological patterns that can induce [24] but also normalize [25,26] cancer. Bioelectric signals regulate not only the single-cell fate such as stem cell differentiation [27,28] but also multicellular properties like size in zebrafish appendages [29] and planarian heads [30], as well as polarity characteristics such as the left-right [16] and anterior-posterior [31,32] axes. While instructive roles for these patterns have been shown in a number of systems [10,12], significant open questions remain about the dynamics underlying the origin, stability, and time-dependent changes in bioelectric patterns.

*smafe@uv.es

In order to understand the establishment and control of bioelectrical patterns, simple models that provide useful metaphors can complement the analysis of specific data obtained in real systems [5]. In a previous study, we considered the stabilization of cell states in the context of genetic networks and multicellular oscillations [33]. Here, we have put emphasis on the effect of the single-cell state on the intercellular coupling, conducting multicellular simulations aimed at describing a range of bioelectrical community effects. The simulations permit us to establish under which conditions a local heterogeneity consisting of, e.g., a small patch of polarized (high absolute value of V) cells can be stabilized against a surrounding depolarized (low absolute value of V) region in different bioelectrical scenarios. It is important to note that all cells are modeled as identical in the sense that they have the same single-cell bioelectrical parameters, the only difference being their distinct (polarized or depolarized) initial states.

The central assumption of the model is that the intercellular voltage-gated gap junctions allow a domain of cells to share the *same* polarization state because of the *high* junction conductances allowing the intradomain connectivity. On the contrary, the intercellular junctions can effectively isolate adjacent domains with *different* polarization states because of the *low* junction conductance and *interdomain* connectivity [4,5]. Because of this *asymmetry*, instructive bioelectrical information can be encoded in spatially separated domains of cells with defined polarization states [3–5]. These slow, quasistationary cell polarization dynamics is to be compared with the fast action potentials transferring information in groups of neurons [3,7,8] where individual cell polarization-depolarization transitions, intercellular connectivity, and multicellular patterns are also involved but differences arise concerning the information processing times and responses. Here we will focus on stationary patterns; oscillatory phenomena regulated by a dynamic intercellular connectivity have also been studied elsewhere [9].

The model simulations discussed here are qualitatively guided by the following experimental facts:

(i) The spatial patterns of identical cells in different states that play an active role in multicellular development can be established not only by extensive spatial gradients of biochemical agents, but also by local fluctuations in gene expression [34,35]. For instance, in a quasihomogeneous distribution of pluripotent cells randomly distributed throughout different phases, the cell cycle constitutes a source of dynamic heterogeneity that can contribute to multicellular patterning [34].

(ii) Differentiated cells tend to be polarized and the completion of differentiation appears to be concomitant with an increase in the intercellular communication [14,34,36]. In this way, local increases in the intercellular connectivity can support the transport of small molecules that allow phenotypic-compartmentalization. Since the intercellular diffusion of signaling agents depends on this connectivity, biochemical and bioelectrical patterns can be interrelated [5,10].

(iii) Gap-junction-coupled multicellular ensembles can show N-shaped current-voltage curves and bi-stability [37,38] at the single-cell level. Experimentally, this characteristic allows quasistatic different electrical domains that coexist at the multicellular level, both in biological and engineered tissues [3,14].

(iv) Vertebrate gap junctions are also voltage-gated: their conductances depend on the cell potential V as well as on the intercellular potential difference, showing high conductances when two adjacent cells have similar V values but low conductances when these cells are in different polarization states [5,10,39–41].

We believe that a description of the basic mechanisms involved in multicellular bioelectrical patterning [5,13,14] can contribute to the understanding of the signals that trigger regeneration and the formation of new organs [3,10,19] as well as to the electroceutical correction of abnormally depolarized regions initiated in the bulk of normal tissues [20,38,42]. While the above cases concern bioelectrical patterns in natural systems, theoretical models can also suggest particular mechanisms for the establishment of target patterns in multicellular engineering [3]. Indeed, if the cell fate is not terminal and there exist epigenetic barriers that can be manipulated via bioelectrical stimuli, individual cellular reprogramming could benefit from the community effects provided by multicellular coupling [5].

II. BIOPHYSICAL MODEL

The biophysical model used in the simulations has been described in detail previously [4,5]. For the sake of simplicity, we have considered a relatively low number of cells and ignored the transcriptional regulation of the single-cell ion channel conductances. This simplifying assumption results in fast time responses of the order of seconds [4,43,44] instead of the comparatively slow responses of the order of hours characteristic of the simulations including diffusional [45] and transcriptional processes [9] with a large number of cells. Note that we have considered previously these long-time phenomena for the case of microRNA diffusion [45] and ion channel protein transcription [9], showing that bioelectrical patterns are coupled to the biochemical ones [9,34,45–48].

The dependence of the gap junction conductance on the single-cell potential V is fully taken into account by introducing an effective conductance $G^o(V)$ that reflects the influence of V on transcription, trafficking to the membrane, and subsequent insertion of the specific connexin protein. This phenomenological approach indirectly incorporates the experimental facts that the loss of pluripotency to differentiation is concomitant with the transition from a depolarized to a polarized cell state and that this transition eventually leads to an increase in the intercellular connectivity [14,34,36].

To better understand the basic model characteristics [4,5], Figs. 1 (*depolarized* cell) and 2 (*polarized* cell) show schematically the two *dep* and *pol* ion channels [37,49], together with the resulting N-shaped current-voltage curves and cell potential bistability [37,38], obtained at the single-cell level. Note that the proliferating state is associated with the depolarized cell whose bioelectrical response is dictated by the *dep* channel (Fig. 1) while the quiescent state is associated with the polarized cell whose response is dictated by the *pol* channel (Fig. 2) [49,50,51–53]. Also, the gap junction conductance between two adjacent depolarized cells is low (Fig. 1) as opposed to the case of two adjacent polarized cells (Fig. 2),

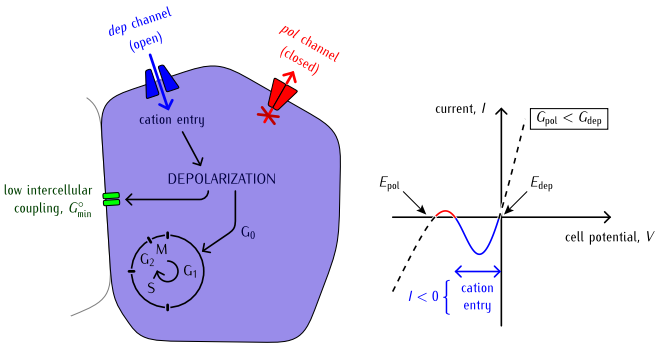

FIG. 1. Schematic view of the model depolarized cell (*left column*) whose potential is governed by two generic voltage-gated channels of maximum conductances G^o_{pol} (*pol* channel acting to polarize the cell potential at values close to the equilibrium potential E_{pol}, *red color on line*) and G^o_{dep}(*dep* channel acting to depolarize the cell at potentials close to E_{dep}, *blue color on line*) [37,38]. The respective inward and outward rectifying channels allow the transitions between two stable polarized and depolarized cell states. The current (I) voltage or cell potential (V) curve (*right column*) shows the case of the dominant *dep* channel where the cation (e.g., Na^+ and Ca^{2+} [49]) entry leads to cell depolarization (*continuous blue curve*), cell cycle entry into G_1 phase, and low intercellular coupling with a minimum junction conductance G^o_{min} (*green color on line*). The scheme shows that the cell cycle phase and the bioelectrical cell state are related [49,51,52]. The model voltage-gated conductances have been studied with detail previously and lead to a cell potential dominated by the ratio G^o_{dep}/G^o_{pol} for constant potentials E_{dep} and E_{pol} [37] in the case of an isolated cell. For multicellular aggregates, however, the effect of intercellular coupling leads to more complex dynamics, as we will show later.

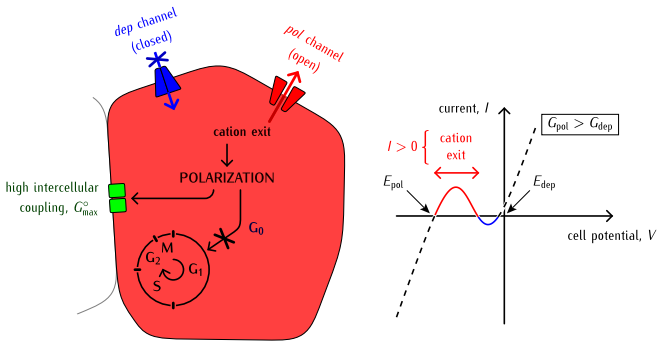

FIG. 2. Schematic view of the model polarized cell (*left column*) and the I–V curve (*right column*) for the case of the dominant *pol* channel [38] where the cation (e.g., K^+ [49]) exit leads to cell polarization (*continuous red curve*), potentials close to E_{pol} rather than to E_{dep}, cell cycle arrest in the G_0 phase [49], and high intercellular coupling with a maximum junction conductance G^o_{max} (*green color on line*).

which is characterized by a high intercellular coupling. In the simulations, we consider an intermediate case between that of Figs. 1 (dominance of depolarized state) and Fig. 2 (dominance of polarized state) for all cells in the multicellular aggregate.

Note that the cell cycle shows rich and complex biochemical dynamics where ion channels play only a partial role [49,51,52] and thus Figs. 1 and 2 do not attempt to give a description of this cycle. Instead, the schemes included for the cycle phases merely suggest that the cell potential V can influence the different phases, e.g., through the voltage-gated transport of signaling ions and molecules [3,5,49,51]. Also, we assume in Figs. 1 and 2 that this V is determined by only two voltage-gated channel populations of effective maximum conductances G^o_{dep} and G^o_{pol} [38]. Experimentally, a variety of ion channels can be found in most cells [54]. However, the fact is that voltage-gated channels are central to cell bioelectricity because the counteracting dynamics of a small number of these channels regulate important physiological functions such as pacemaking mechanisms, circadian clocks and the cell cycle, slow-wave oscillations in neurons, and bioelectrical oscillations in engineered tissues [5].

In the simulations, we use the following phenomenological equations that qualitatively describe the main experimental features of the I–V curves of voltage-gated channels [38,54]:

$$I_{dep} = G_{dep}(V - E_{dep}) = \frac{G^o_{dep}(V - E_{dep})}{1 + \exp[-z(V - V_{th})/V_T]}, \quad (1)$$

$$I_{pol} = G_{pol}(V - E_{pol}) = \frac{G^o_{pol}(V - E_{pol})}{1 + \exp[z(V - V_{th})/V_T]}, \quad (2)$$

where we have written explicitly the dependence of the voltage-gated conductances G_{dep} and G_{pol} on the cell potential V [54]. Typical channels parameters are $G^o_{dep}/G^o_{pol} = 1.5$ for the conductance ratio, $z = 3$ for the channel gating charge, and $V_{th} = -V_T = -(RT/F)$ for the threshold potential, where R is the gas constant, T is the temperature, and F is the Faraday constant [4,5,54]. Also, we introduce the generic values $E_{dep} = 0$ mV and $E_{pol} = -60$ mV for the equilibrium *dep* and *pol* potentials, respectively [4,54]. For this choice of parameters, an isolated cell is in a bistability regime [38] intermediate between that of Figs. 1 and 2. This regime shows rich bioelectrical dynamics, with two stable resting potentials at around -57 mV (polarized cell solution) and -3 mV (depolarized cell solution). Between these stable potentials, an unstable potential around -32 mV divides the potential range into the polarized ($V < -32$ mV) and depolarized states ($V > -32$ mV), as shown schematically in the I–V curves of Figs. 1 and 2.

Experimentally, each pair of neighboring cells i and j are coupled by voltage-gated gap junctions that allow a dynamic plasticity at the multicellular level. Figs. 3(a)–3(c) describe the possible states of the resulting intercellular gap junction conductance G_{ij}. It is important to note that G_{ij} shows different dependences on the electric potential:

(i) At the single-cell level, the *individual* junction conductance of cell i is a function $G^o_i[V_i]$ of the cell potential V_i [Fig. 3(a)]. Polarized cells tend to show higher intercellular couplings than depolarized cells [14,34,36], as shown schematically in Fig. 3(b). We use the following

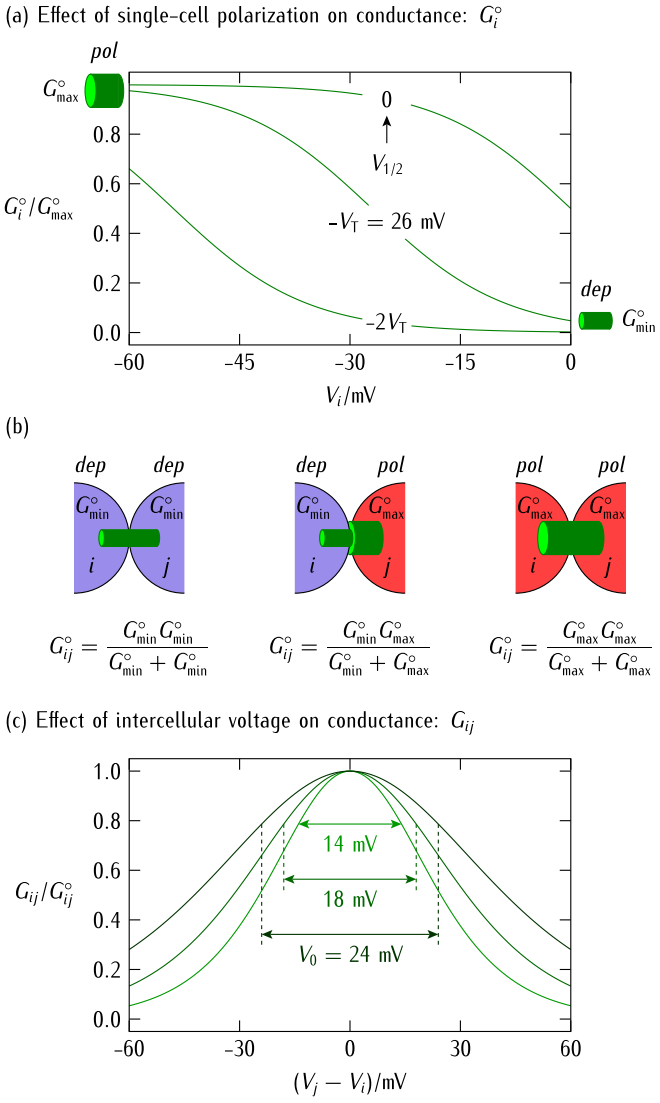

FIG. 3. The single-cell (*individual*) junction conductance G_i^o as a function of the potential V_i and parametrically in $V_{1/2}$ [Eq. (3)] varies between the maximum value G^o_{max} for the case of a fully polarized cell and a minimum value G^o_{min} for a depolarized cell (a). The *intercellular* junction conductance $G^o_{ij} = G^o_i G^o_j/(G^o_i + G^o_j)$ of Eq. (4) for two adjacent cells i and j of individual junction conductances G^o_i and G^o_j depends on the respective potentials V_i and V_j. The scheme shows the limiting cases of low G^o_{min} and high G^o_{max} conductances (b). In addition, the gap junction conductance G_{ij} between cells i and j is also voltage-gated and follows a bell-shaped function of the potential difference $V_i - V_j$(intercellular voltage) that is shown parametrically in V_0 (c). The junction parameters $V_{1/2}$ and V_0 allow to reproduce qualitatively a range of experimental shapes observed for the conductances of different junction proteins [5,39–41].

phenomenological function in Fig. 3(a):

$$G^o_i = \frac{G^o_{max}}{1 + \exp[\alpha(V_i - V_{1/2})/V_T]}, \tag{3}$$

where G^o_{max} is the maximum conductance, α is a parameter that controls how steep is the change of G^o_i with V_i, $V_{1/2}$ is a reference cell potential at which $G^o_i = G^o_{max}/2$, and $V_T = 26$ mV approximately [4]. Note that the conductance of Eq. (3) decreases with the absolute value of the cell potential: the maximum value G^o_{max} corresponding to a polarized cell decreases to a generic minimum value G^o_{min} of a depolarized cell [Fig. 3(a)].

(ii) At the multicellular level, the maximum *intercellular* junction conductance reflecting the coupling between two adjacent cells is defined from the series arrangement of the *individual* junction conductances [Fig. 3(b)] because the gap junction is formed from neighboring connexon hemichannels [34]. In this way, the cell cycle dynamics can produce an intercellular heterogeneity [34] because of the different individual junctions of depolarized (Fig. 1, *green color on line*, minimum conductance) and polarized (Fig. 2, *green color on line*, maximum conductance) cells; see also Figs. 3(a) and 3(b). This intercellular heterogeneity eventually contributes to the multicellular electrical regionalization, as we will show later.

(iii) Experimentally, function $G_{ij}[(V_i - V_j)]$ depends on the variable $(V_i - V_j)$ because the *intercellular* conductance between two adjacent cells i and j of respective potentials V_i and V_j is voltage gated [Fig. 3(c)]:

$$G_{ij} = \frac{2G^o_{ij}}{1 + \cosh[(V_i - V_j)/V_0]}, \quad G^o_{ij} = \frac{G^o_i G^o_j}{G^o_i + G^o_j}, \tag{4}$$

where V_0 is a parameter that controls how wide is the bell-shaped conductance G_{ij} as a function of the potential difference $V_i - V_j$. Equation (4) qualitatively reproduces the experimental shapes obtained in different gap junctions [39–41]. Note that the intercellular junction conductance of Eq. (4) depends also on the individual potentials V_i and V_j of cells i and j [Fig. 3(a)]. In this way, the dynamic network of coupled cells can be regulated both at the single-cell transcriptional level [Eq. (3)] and at the intercellular post-translational level [Eq. (4)].

Note that Eqs. (3) and (4) constitute only an approximate approach to the complex problem of connexin transcription, trafficking to the membrane, and subsequent insertion of the respective connexons in two neighboring cells to form the gap junctions. Because of the functional dependence of G_{ij} on both the individual potentials V_i and V_j [Eq. (3) and Fig. 3(a)] and their difference $V_i - V_j$ [Eq. (4) and Fig. 3(c)], the maximum of the intercellular gap junction conductance is achieved when both cells are in the polarized state [Fig. 3(b)]. However, the maximum of the intercellular current $I_{ij} = G_{ij}(V_j - V_i)$ is obtained when one cell is in the polarized state (about -60 mV in our simulations) and the other neighboring cell is in the potential region just before the transition from high to low values of G^o_i [Fig. 3(a)] so that the individual junction conductances are high but the potential difference $(V_j - V_i)$ is nonzero. The phenomena arising from this multicellular coupling are the main objective of the simulations presented.

At the whole ensemble level, each cell potential V_i changes with time t because of (i) the I_{dep} and I_{pol} channel currents of Eqs. (1) and (2) and (ii) the intercellular current I_{ij} across the junction conductances of Eqs. (3) and (4) [5]:

$$C_i \frac{dV_i}{dt} = -I_{dep} - I_{pol} + \sum_{\substack{j \in \text{nearest} \\ \text{neighbors}}} G_{ij}(V_j - V_i). \tag{5}$$

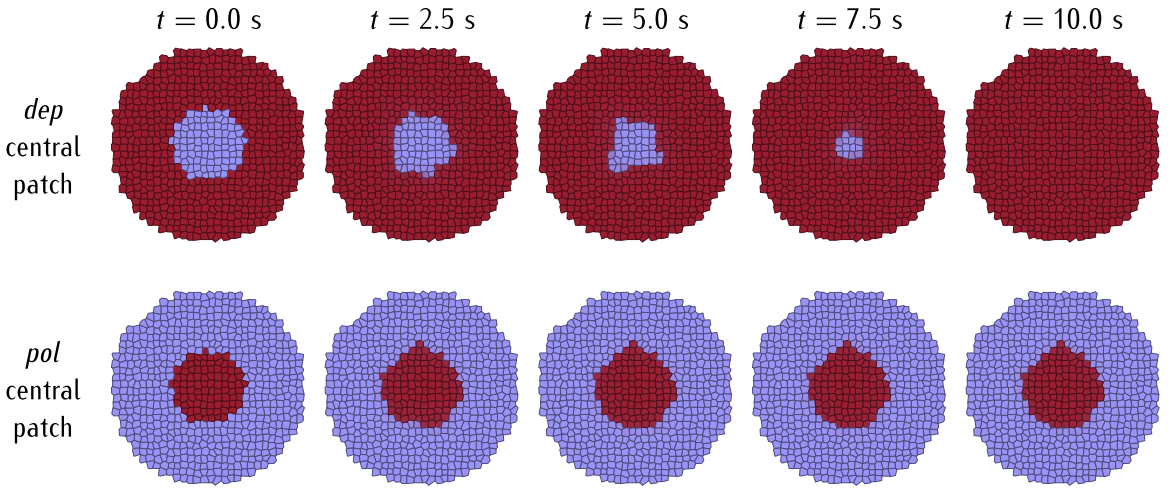

FIG. 4. Time evolution of the multicellular ensemble for two polarizations of the central patch, with $n(\text{patch}) = 91$ and $N(\text{ensemble}) = 642$ cells. The parameters used for the intercellular gap junctions in Eqs. (3) and (4) are $G^o_{\max} = 1.5G_{\text{ref}}$, $\alpha = 3$, $V_0 = 24\,\text{mV}$, and $V_{1/2} = 30\,\text{mV}$. Because the community effect is more intense for the polarized cells than for the depolarized ones, as shown by the different intercellular couplings of Fig. 3(b), a depolarized patch cannot resist conversion by the polarized bulk (*top row*). On the contrary, a polarized patch can resist conversion by the depolarized surrounding bulk, thus establishing a persistent bioelectrical regionalization in the ensemble (*bottom row*). Note that this regionalization is electrically assisted by the junction conductances of Eqs. (3) and (4) that increase with cell polarization.

In the simulations, we introduce an average number of four neighbor junctions around each central cell. For an individual cell capacitance $C_i = 100\text{pF}$ and a channel reference conductance $G^o_{\text{ref}} \equiv G^o_{\text{pol}} = 1\text{nS}$, the characteristic time $\tau = C_i/G^o_{\text{ref}} = 0.1\text{s}$ is obtained for the cell bioelectrical state. In the case of a multicellular ensemble composed of hundreds of cells, however, this time can be of the order of tens of seconds [4,5,43,44].

III. RESULTS AND DISCUSSION

Spatial heterogeneities composed of identical cells in different states are characteristic of development and function [3,5,34,35,47] and can be established by gradients of diffusible molecules [46,47] and local fluctuations in gene expression [34,35]. In the simulations, we assume a local heterogeneity consisting of a small number of cells (*patch*) whose local polarization state differs from that of the surrounding bulk at time $t = 0$ and let the multicellular ensemble evolve for different coupling conditions (Fig. 4). This initial bioelectrical heterogeneity might arise because of a locally different complement of voltage-gated channels giving distinct effective conductances G^o_{dep} and G^o_{pol} or a local fluctuation in the ionic concentrations giving distinct equilibrium potentials E_{dep} and E_{pol}; see Figs. 1 and 2. However, we introduce here the *same parameters* for all individual cells in the aggregate and take profit of the cell bistability to set initially *different cell states* in the two regions of Fig. 4. We emphasize that this procedure permits us to ascribe the observed effects to the distinct intercellular couplings of Fig. 3(b) rather than to the specific characteristics of a particular cell because all single-cell parameters are identical. In this way, the simulations can complement the cell-centered view with multicellular community concepts, with an emphasis on bioelectrical effects.

It is important to note first the time scale of the simulations: while multicellular regionalization can be a slow process, the fact is that the relatively fast establishment of electrical patterns can influence the subsequent long time diffusional and transcriptional processes [3,5,12,46,47], as mentioned in the above section. Here, we focus on the electrical relaxation of a small number of cells and no attempt is made to describe those phenomena that occur at much longer times along the established bioelectrical patterns [9,38,45]. Experimentally, these patterns can act as templates for the spatiotemporal distributions of signaling ions and molecules that modulate other downstream biochemical processes over real systems with a large number of cells [3,20,43,55].

Initially, we take every isolated cell in the ensemble to be in one of the two stable potentials characterizing the *dep* (Fig. 1) and *pol* (Fig. 2) states. Because of the experimental significance of the cell polarization in bioelectricity, we consider two generic cases in Fig. 4: a depolarized bulk ensemble with a polarized central patch and a polarized bulk ensemble with a depolarized patch. At time $t > 0$, we describe the time evolution of the multicellular system that is ruled by the feedback between the evolving single-cell states (Figs. 1 and 2) and the dynamic intercellular connectivity (Fig. 3).

From a purely bioelectrical view, the destabilization of the initially depolarized patch by a polarized surrounding bulk (Fig. 4, *top row*) could be interpreted as a control procedure avoiding local depolarization and subsequent proliferation in a quiescent multicellular ensemble. On the contrary, the eventual stabilization of the polarized patch in a depolarized surrounding bulk (Fig. 4, *bottom row*) would suggest a bioelectrically assisted local polarization and differentiation. While we are aware of the biological complexity of these phenomena in real systems, we believe also that the above bioelectrical views can provide complementary and useful insights to the current biochemical descriptions.

Figure 5 shows the final state of the multicellular ensemble reached after the bioelectrical relaxation for the two initial states of Fig. 4 and different values of the maximum

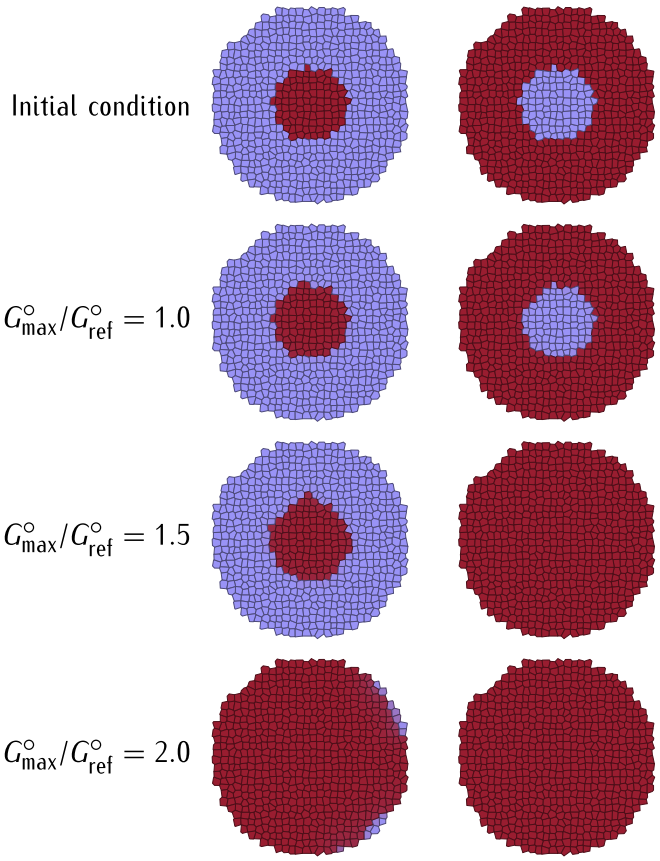

FIG. 5. Final states of the cell ensemble at time $t = 20$ s for different values of the coupling intercellular conductance G^{o}_{max}/G^{o}_{ref} and the cases of the *pol* (*left column*) and *dep* (*right column*) central patches shown in Fig. 4. The rest of parameters controling the gap junction conductance are those of Fig. 4. In the multicellular case, the depolarized and polarized single-cell states of Figs. 1 and 2 are modulated not only by the channel conductances ratio G^{o}_{dep}/G^{o}_{pol} and the potentials E_{dep} and E_{pol} [Eqs. (1) and (2)] but also by the junction conductances of Fig. 3 [Eqs. (3) and (4)].

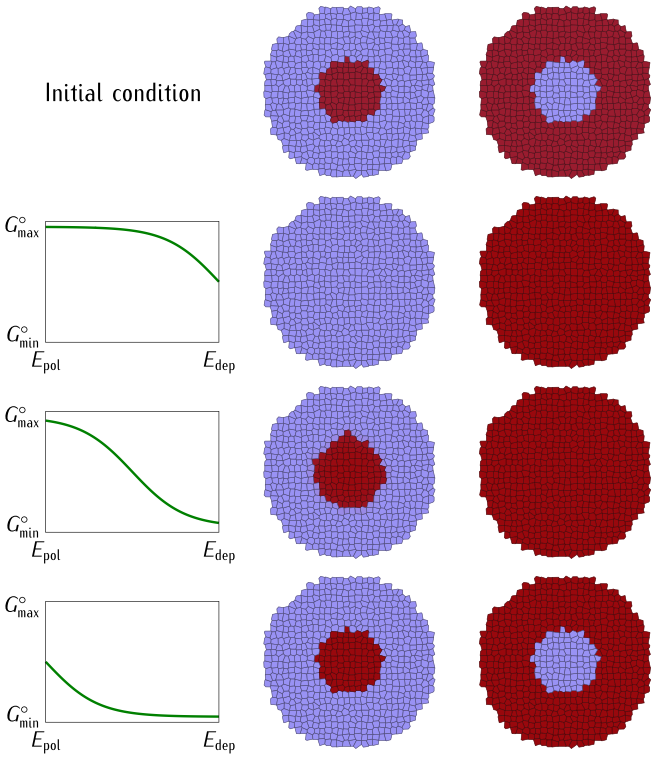

FIG. 6. Initial conditions and different final states of the multicellular ensemble obtained for different values of $V_{1/2}$ in Eq. (3), with $G^{o}_{max}/G^{o}_{ref} = 1.5$ and the same initial conditions as in Fig. 5. The rest of the parameters that control the gap junction conductance are those of Fig. 4. At $V_{1/2} = 0$ mV(*top row* after the initial condition), the central patch is converted by the surrounding bulk irrespective of the initial condition because of the relatively high junction conductances of Fig. 3(a). At negative values $V_{1/2} = -30$ mV (*intermediate row*), however, the community effect becomes weaker, especially for depolarized cells, because of the low junction conductances achieved. Eventually, this effect vanishes for sufficiently negative values $V_{1/2} = -60$ mV (*bottom row*) giving very low junction conductances. The *left column* schematically shows the conductance G^{o}_{i} as a function of the cell potential V_i for the three cases of $V_{1/2}$ considered.

junction conductance G^{o}_{max}. This conductance is a measure of the coupling degree between neighboring cells [Fig. 3(b)] that depends on the single-cell potential and polarization state [Eq. (3) and Fig. 3(a)]. Clearly, a low value of G^{o}_{max} corresponding to a depolarized state gives an essentially isolated cell whose individual dynamics cannot be controlled by the intercellular coupling while a high value of G^{o}_{max} gives an isopotential ensemble where no bioelectrical information associated with a specific regionalization can be encoded.

For low values of G^{o}_{max}, the intercellular coupling is weak both for polarized and depolarized cells, and thus the initial states of Fig. 5 can persist over time for the two patches. For high intercellular coupling, however, even the depolarized cells in the bulk can eventually be converted to the polarized state of Fig. 2 because of the dominance of the intercellular coupling in the case of polarized cells [Fig. 3(b)]. Note that it is the intermediate value of G^{o}_{max} that permits both the destabilization of the depolarized patch (Fig. 5, *right column*) and the stabilization of the polarized patch in a depolarized surrounding bulk (Fig. 5, *left column*). Although differentiation involves complex biochemical phenomena that occur over a variety of time scales [34,48], it is tempting to speculate that the locally persistent polarized state characteristic of differentiated cells could be bioelectrically facilitated by the high *intradomain* coupling [Figs. 3(b) and 5, *left column*]. On the contrary, the existence of a depolarized patch within a polarized surrounding bulk is difficult (Fig. 5, *right column*) because of the low *intradomain* coupling [Fig. 3(b)], thus suggesting that bioelectrical phenomena could also contribute to the control of local depolarization and cell proliferation in a polarized and quiescent multicellular ensemble.

Figure 6 shows the effect of the reference potential $V_{1/2}$ on the individual junction conductance G^{o}_{i} of Eq. (3). For low absolute values of $V_{1/2}$ (Fig. 6, *top row* after the initial condition), this conductance takes high values close to G^{o}_{max} over most of the cell potential V_i range [Fig. 3(a)] so that the strong community effect exerted by the majority of cells in the surrounding bulk on the small central patch eventually leads to an isopotential ensemble for the two initial conditions considered. As $V_{1/2}$ takes higher absolute values (Fig. 6, *intermediate*

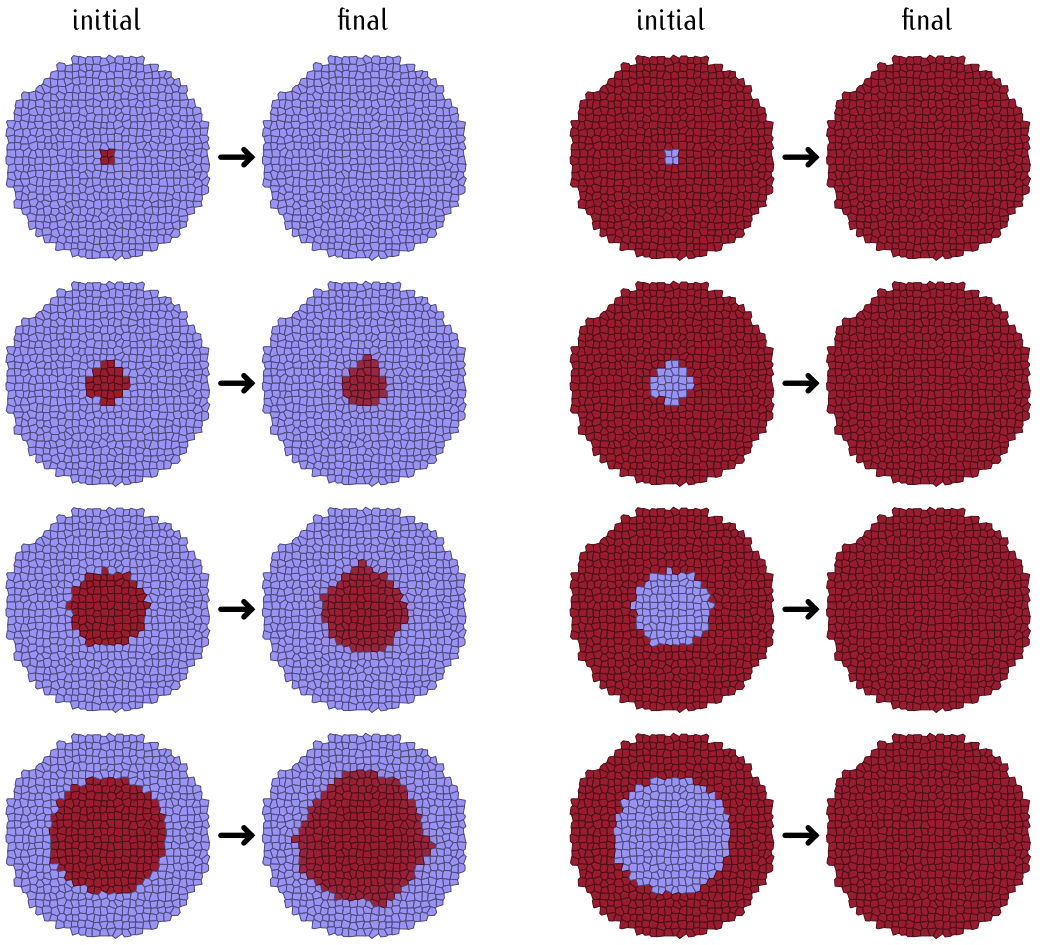

FIG. 7. The multicellular ensemble time evolution for different patch sizes and the same parameters of Fig. 4. The weak dependence on the patch size is explained here by the dominance of the polarized state caused by the increased gap junction conductance [Eq. (3) and Figs. 3(a) and (b)] together with the nearest-neighbor condition of Eq. (5). The community effect caused by the depolarized bulk on the polarized patch is apparent only for very small patch patches (*left column*). On the contrary, the depolarized patch evolves toward a fully polarized one irrespective of its the size (*right column*). This asymmetry emphasizes again the different junction dynamics of polarized and depolarized cells whose single-cell parameters are identical, thus suggesting a possible bioelectrical asymmetry of differentiated and proliferating cells, respectively.

row), however, G_i^o decreases significantly with V_i [Fig. 3(a)] and thus the above community effect becomes weaker so that the central polarized patch can resist depolarization by the surrounding bulk. This is not the case of the depolarized central patch surrounded by a polarized bulk where no spatial regionalization can now be maintained because of the *asymmetry* in the coupling degree experienced by polarized and depolarized cells [Fig. 3(b)].

As $V_{1/2}$ moves further to more negative values (Fig. 6, *bottom row*), no community effect caused by the surrounding bulk on the central patch can occur because of the low values attained by the coupling conductance G_i^o [Fig. 3(a)]. Thus, the initial electric potential regionalization can now be maintained with time for the two cases of Fig. 6. Note that low conductances G_i^o give also low intercellular currents $I_{ij} = G_{ij}(V_i - V_j)$ [Figs. 3(b) and3 (c)], which makes it difficult to orchestrate bioelectrical changes in the now persistent ensemble state. The different spatial regionalizations obtained in Fig. 6 clearly show the richness of the biophysical situations that can be described by the dynamic intercellular coupling model despite its apparent simplicity, as emphasized previously in a variety of experimental cases [4,5].

Figure 7 shows the effect of the central patch size on the ensemble time evolution in the two cases considered in the simulations. For the range of biophysical parameters used, the system evolution is dictated by the bistability of the cell state (Figs. 1 and 2) and the fact that the intercellular junction conductance is higher, and thus the intercellular coupling is stronger, when the adjacent cells are polarized (Fig. 3), which explains the asymmetry observed in the community effects of Fig. 7: small polarized patches can resist depolarization (*left column*) but depolarized patches cannot resist polarization even for large sizes (*right column*).

To better show the patch size and spatial distribution effects on potential regionalization, Fig. 8 (*bottom row*) shows the time evolution of separated groups of cells initially in the polarized state compared with the case of a polarized central patch (Fig. 8, *top row*). As expected, the community effect of the depolarized surrounding bulk on the polarized patches is weak only for sufficiently large patches. Note however

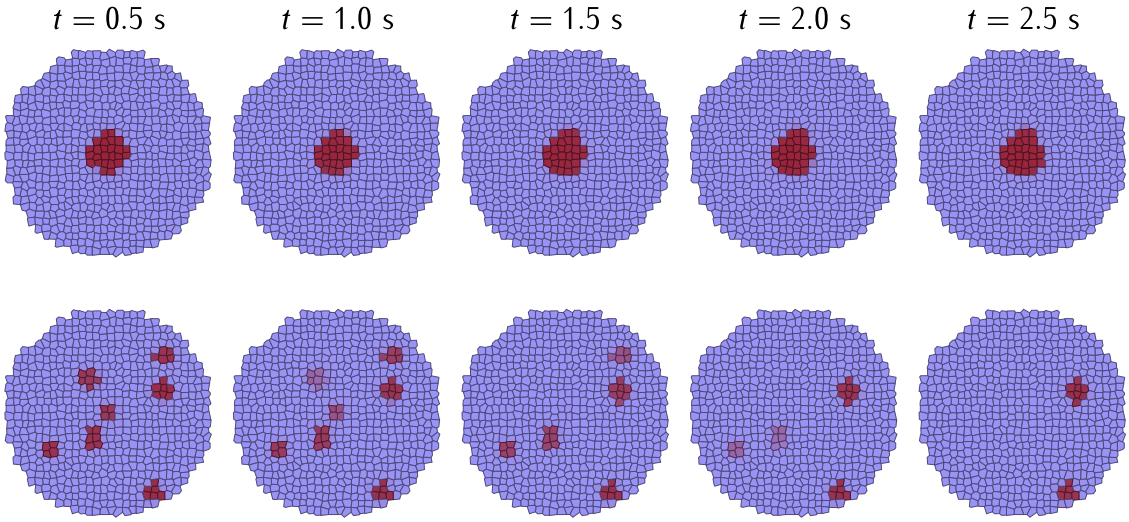

FIG. 8. Time evolution of the multicellular ensemble for the cases of a unique central patch (*top row*) and multiple small patches (*bottom row*) for the same parameters of Fig. 4. While the number of polarized cells in the *top row* panel is actually lower than that in the *bottom row* panel, the community effect caused by the depolarized bulk is more significant in the second case, suggesting that the number of cells in the patch and its particular location in the ensemble are crucial for the system evolution.

that although the initial number of polarized cells is actually higher in the *bottom row* panel than in the *top row* panel, their fragmented arrangement in very small patches significantly weakens the community effect so that the bulk of depolarized cells is now able to convert a number of small polarized patches.

Note that according to the results of Fig. 7 (*right column*), the bioelectrical normalization effect displayed in the *bottom row* panel of Fig. 8 should be even more marked for the case of *depolarized* rather than polarized multiple spots (not shown in the Fig.). This model prediction can be related to different experimental phenomena [19,26]. When additional eye foci are induced all over the body in frog embryogenesis by means of the misexpression of ion channels and the ectopic expression of eye induction genes such as Pax6 and Rx1 is examined, a progressive reduction in the number of positive spots is seen over developmental time; the neighboring tissue tends to suppress ectopic eye fields [19]. Similarly, ectopic spots of depolarization often do not become tumors due to the bioelectrical-normalizing action of their neighbors [26,38].

Experimentally, changes in the single-cell state can initiate a redistribution of connexins within a cell population and thus modify the intercellular connectivity [34,36]. Figures 4 –8 suggest different bioelectrical mechanisms that are based on *two experimental facts*: the cell polarization state influences the expression and function of the junction proteins and the intercellular conductances are small at the interface between polarized and depolarized regions (Fig. 3). In this way, the dynamic voltage-gated intercellular connectivity emerges as a regulatory mechanism that can permit or suppress a local bioelectrical heterogeneity within a multicellular ensemble of identical cells.

Note that the electric potential and intercellular connectivity regionalizations establish preferential paths and directions for the transport and distribution of the signaling ions and molecules [3,20,34] that may eventually trigger locally different cell states and processes [34,47]. In this way, spatial patterns of electric potentials can be regarded as prepatterns for the concentration of signaling agents with the advantage of allowing efficient connection between distant regions of a multicellular aggregate. The transport phenomena of these chemical agents and their subsequent feedback effects on growth, development, and regeneration are not described in the present simulations, which are instead focused on the establishment of bioelectrical patterns by the dynamic network of voltage-gated ion channels and intercellular junctions [3,5]. New model systems and simulations can now address how these outcomes are affected by the transport of these biochemical agents or by the external insertion of small multicellular patches of a defined bioelectrical state into large hosts.

Also, bioelectrical patterns usually involve symmetry breaking and subsequent amplification effects. Thus, the establishment of large-scale bioelectric circuits should certainly depend on the tissue dimensionality. We have so far analyzed two-dimensional (2D) model tissues and 1D linear chains of multicellular aggregates [4,5]. However, it is reasonable to expect that extending the simulations into the 3D space should give significant community effects because of the increase in the number of neighboring cells that can influence the bioelectrical state of a central cell and future efforts can consider this extension.

Importantly, the results of Figs. 3(a) and 3(c) for the intercellular gap junctions together with the schemes of Figs. 1 and 2 for the single-cell bioelectrical bistability immediately suggest a possible mechanism for the establishment of memories based on spatial electrical patterns. Indeed, the gap junctions that couple two neighboring cells are reminiscent of *synapses* whose strength depends on both the individual cell i state [potential V_i in Fig. 3(a)] and its relative state with respect to the neighbor cell j [intercellular potential $V_i - V_j$ in Fig. 3(c)], showing thus plasticity characteristics [56,57]. In this way, the model predicts that spatial patterns of electric potentials to be decoded as morphological outcomes [3,5] can be established by the combined action of the individual cell bistable

contribution to the intercellular synapsis and its reinforcement when two neighboring cells share the same bioelectrical state [Fig. 3(b)], which allows the synchronization of multicellular aggregates sharing the same bioelectrical state, as described previously [9]. The above single-cell and intercellular combined control shows qualitative similarities to the case of networks composed by excitable cells. For instance, there are ways to modify the state of a neuron other than acting on synapses because changes in specific ion pumps and channels may influence the cellular excitability. In addition, the post-translational modification of intercellular coupling shown in Fig. 3(c) is reversible and provides thus a plasticity that can be modulated by the bioelectrical states of neighboring cells [4,5].

IV. CONCLUSIONS

The model simulations suggest bioelectrical mechanisms to influence the single-cell fate by using the dynamic coupling with the neighboring cells. In particular, community effects can allow the reprogramming of single-cell bioelectrical states by the spatiotemporal correlation of cell potentials at the multicellular level, in agreement with recent experimental data [3,12,20,42,55]. In our case, these effects emerge from a delicate balance between the degrees of intercellular coupling in: (i) the central patch, (ii) the surrounding bulk, and (iii) the interface that separates these two regions.

We emphasize that all cells used in the simulations are *identical* and share the same single-cell parameters. The different cell fates described by the polarized state, reminiscent of quiescent cells, and the depolarized state, reminiscent of proliferating cells [50–52], are established by the distinct community effects of Fig. 3(b). In this way, a strongly interconnected polarized patch can resist depolarization by a weakly interconnected depolarized bulk, which may constitute a bioelectrical mechanism to consolidate local polarization changes. Conversely, the opposite effect should be much weaker because the strongly interconnected polarized bulk will tend to convert a weakly interconnected depolarized patch, which suggests a mechanism to control proliferating patches in a quiescent bulk. This mechanism may, however, fail if the interfacial coupling weakens, as it occurs in the initial tumorigenesis phases [38,58,59]. Note that we do not claim here that the individual cell characteristics are irrelevant in real cases. Rather, we have introduced identical cells only to emphasize community effects in the aggregate, suggesting thus that the bioelectrical coupling is also crucial [3,5].

While cell potentials could not be considered transcription factors themselves, they can still influence transcription via other biochemical and mechanical downstream processes [1–3,5,10–12]. Note that genetics and bioelectricity are coupled: the genes code for ion channel and gap junction proteins, these proteins regulate the cell bioelectricity and, in turn, bioelectrical signals influence downstream gene expression, thus closing the feedback loop. We suggest here that this feedback can be extended from the single-cell description of Figs. 1 and 2 to the multicellular patterns of Figs. 4–8 because of the intercellular coupling of Fig. 3. These patterns are important not only for the understanding of development and regeneration but also for replicating morphogenic processes in engineered multicellular systems [3,35]. Note in this context that the building blocks used in the model simulations are amenable to external modulation: the proteins forming the single-cell ion channels and the intercellular gap junctions can be regulated at the transcription, translation, and post-translational levels, e.g., by mRNA microinjection, blocking by specific ions and molecules, and optical pulses [3,12–14,34,42,45,54,60]. On the basis of these experimental facts, we believe that bioelectrical patterns should be good candidates for operational control because in addition to encode instructive information that is eventually decoded as biological outcomes [3–5,12,20], they involve multicellular potentials rather than molecular characteristics of the individual cell. In this context, the simulations show clearly how physical models can contribute to the understanding of complex bioelectrochemical involving cellular aggregates [5] and electroactive biofilms [61,62].

ACKNOWLEDGMENTS

J.C., P.R., and S.M. acknowledge the Ministerio de Ciencia e Innovación (Spain) and the European Regional Development Funds (FEDER), Project No. PGC2018-097359-B-I00. M.L. acknowledges the support by an Allen Discovery Center award from The Paul G. Allen Frontiers Group (No. 12171), the Templeton World Charity Foundation (TWCF0089/AB55), the Barton Family Foundation, and the Defense Advanced Research Projects Agency (DARPA) under Cooperative Agreement Number HR0011-18-2-0022 (the content of the information does not necessarily reflect the position or the policy of the Government, and no official endorsement should be inferred).

[1] A. N. Landge, B. M. Jordan, X. Diego, and P. Müller, Pattern formation mechanisms of self-organizing reaction-diffusion systems, Dev. Biol. **460**, 2 (2020).

[2] A. Leronni, L. Bardella, L. Dorfmann, A. Pietak, and M. Levin, On the coupling of mechanics with bioelectricity and its role in morphogenesis, J. R. Soc. Interface **17**, 0177 (2020).

[3] J. Mathews and M. Levin, The body electric 2.0: Recent advances in developmental bioelectricity for regenerative and synthetic bioengineering, Curr. Opin. Biotechnol. **52**, 134 (2018).

[4] J. Cervera, V. P. Pai, M. Levin, and S. Mafe, From non-excitable single-cell to multicellular bioelectrical states supported by ion channels and gap junction proteins: Electrical potentials as distributed controllers, Prog. Biophys. Mol. Biol. **149**, 39 (2019).

[5] J. Cervera, M. Levin, and S. Mafe, Bioelectrical coupling of single-cell states in multicellular systems, J. Phys. Chem. Lett. **11**, 3234 (2020).

[6] R. A. Gatenby and B. R. Frieden, Cellular information dynamics through transmembrane flow of Ions, Sci. Rep. **7**, 15075 (2017).

[7] R. A. Gatenby, The role of cell membrane information reception, processing, and communication in the structure and function of multicellular tissue, Int. J. Mol. Sci. **20**, 3609 (2019).

[8] J. Cervera, A. Pietak, M. Levin, and S. Mafe, Bioelectrical coupling in multicellular domains regulated by gap junctions: a conceptual approach, Bioelectrochem. **23**, 45 (2018).

[9] J. Cervera, J. A. Manzanares, S. Mafe, and M. Levin, Synchronization of bioelectric oscillations in networks of nonexcitable cells: from single-cell to multicellular states, J. Phys. Chem. B **123**, 3924 (2019).

[10] M. Levin, G. Pezzulo, and J. M. Finkelstein, Endogenous bioelectric signaling networks: Exploiting voltage gradients for control of growth and form, Annu. Rev. Biomed. Eng. **19**, 353 (2017).

[11] A. Acardi, Lipids link ion channels and cancer. Membrane voltage connects lipid organizationto cell proliferation, Science **349**, 789 (2015).

[12] J. Mathews and M. Levin, Gap junctional signaling in pattern regulation: Physiological network connectivity instructs growth and form, Dev. Neurobiol. **77**, 643 (2017).

[13] H. M. McNamara, H. Zhang, C. A. Werley, and A. E. Cohen, Optically Controlled Oscillators in an Engineered Bioelectric Tissue, Phys. Rev. X **6**, 031001 (2016).

[14] H. M. McNamara, R. Salegame, Z. A. Tanoury, H. Xu, S. Begum, G. Ortiz, O. Pourquie, and A. E. Cohen, Bioelectrical domain walls in homogeneous tissues, Nat. Phys. **16**, 357 (2020).

[15] S. Manicka and M. Levin, Modeling somatic computation with non-neural bioelectric networks, Sci. Rep. **9**, 18612 (2019).

[16] M. Levin, T. Thorlin, K. R. Robinson, T. Nogi, and M. Mercola, Asymmetries in H+/K+-ATPase and cell membrane potentials comprise a very early step in left-right patterning, Cell **111**, 77 (2002).

[17] D. S. Adams, K. R. Robinson, T. Fukumoto, S. Yuan, R. C. Albertson, P. Yelick, L. Kuo, M. McSweeney, and M. Levin, Early, H+-V-ATPase-dependent proton flux is necessary for consistent left-right patterning of non-mammalian vertebrates, Development **133**, 1657 (2006).

[18] I. Weiß and J. Bohrmann, Electrochemical patterns during Drosophila oogenesis: ion-transport mechanisms generate stage-specific gradients of pH and membrane potential in the follicle-cell epithelium, BMC Dev Biol **19**, 12 (2019).

[19] V. P. Pai, S. Aw, T. Shomrat, J. M. Lemire, and M. Levin, Transmembrane voltage potential controls embryonic eye patterning in Xenopus laevis, Development **139**, 623 (2012).

[20] V. P. Pai, J. Cervera, S. Mafe, V. Willocq, E. K. Lederer, and M. Levin, HCN2 channel-induced rescue of brain teratogenesis via local and long-range bioelectric repair, Front. Cell. Neurosci. **14**, 136 (2020).

[21] V. P. Pai, A. Pietak, V. Willocq, B. Ye, N.-Q. Shi, and M. Levin, HCN2 Rescues brain defects by enforcing endogenous voltage pre-patterns, Nat. Commun. **9**, 998 (2018).

[22] L. N. Vandenberg, D. S. Adams, and M. Levin, Normalized shape and location of perturbed craniofacial structures in the Xenopus tadpole reveal an innate ability to achieve correct morphology, Dev. Dyn. **241**, 863 (2012).

[23] D. S. Adams, S. G. M. Uzel, J. Akagi, D. Wlodkowic, V. Andreeva, P. Cr. Yelick, A. Dewitt-Lee, J.-F. Pare, and M. Levin, Bioelectric signalling via potassium channels: a mechanism for craniofacial dysmorphogenesis in KCNJ2-associated Andersen-Tawil syndrome, J. Physiol. **594**, 3245 (2016).

[24] J. Morokuma, D. Blackiston, D. S. Adams, G. Seebohm, B. Trimmer, and M. Levin, Modulation of potassium channel function confers a hyperproliferative invasive phenotype on embryonic stem cells, Proc. Natl. Acad. Sci. USA. **105**, 16608 (2008).

[25] B. T. Chernet and M. Levin, Transmembrane voltage potential is an essential cellular parameter for the detection and control of tumor development in a Xenopus model, Dis. Model. Mech. **6**, 595 (2013).

[26] B. T. Chernet and M. Levin, Endogenous voltage potentials and the microenvironment: Bioelectric signals that reveal, induce and normalize cancer, J. Clin. Exp. Oncol. Suppl. **1**, S1-002 (2013).

[27] C. Lange, S. Prenninger, P. Knuckles, V. Taylor, M. Levin, and F. Calegari, The H(+) vacuolar ATPase maintains neural stem cells in the developing mouse cortex, Stem Cells Dev. **20**, 843 (2011).

[28] V. Hinard, D. Belin, S. Konig, C. R. Bader, and L. Bernheim, Initiation of human myoblast differentiation via dephosphorylation of Kir2.1 K+ channels at tyrosine 242, Development **135**, 859 (2008).

[29] S. Perathoner, J. M. Daane, U. Henrion, G. Seebohm, C. W. Higdon, S. L. Johnson, C. Nüsslein-Volhard, and M. P. Harris, Bioelectric signaling regulates size in zebrafish fins, PLoS Genet. **10**, e1004080 (2014).

[30] W. S. Beane, J. Morokuma, J. M. Lemire, and M. Levin, Bioelectric signaling regulates head and organ size during planarian regeneration, Development **140**, 313 (2013).

[31] W. S. Beane, J. Morokuma, D. S. Adams, and M. Levin, A chemical genetics approach reveals H,K-ATPase-mediated membrane voltage is required for planarian head regeneration, Chem. Biol. **18**, 77 (2011).

[32] F. Durant, J. Bischof, C. Fields, J. Morokuma, J. LaPalme, A. Hoi, and M. Levin, The role of early bioelectric signals in the regeneration of planarian anterior/posterior polarity, Biophys J. **116**, 948 (2019).

[33] J. Cervera, J. A. Manzanares, and S. Mafe, Cell-cell bioelectrical interactions and local heterogeneities in genetic networks: a model for the stabilization of single-cell states and multicellular oscillations, Phys. Chem. Chem. Phys. **20**, 9343 (2018).

[34] C. M. Glen, T. C. McDevitt, and M. L. Kemp, Dynamic intercellular transport modulates the spatial patterning of differentiation during early neural commitment, Nat. Commun. **9**, 4111 (2018).

[35] E. Nadezhdin, N. Murphy, N. Dalchau, A. Phillips, and J. C. W. Locke, Stochastic pulsing of gene expression enables the generation of spatial patterns in Bacillus subtilis Biofilms, Nat. Commun. **11**, 950 (2020).

[36] W. Yang, P. D. Lampe, P. Kensel-Hammes, J. Hesson, C. B. Ware, L. Crisa, and V. Cirulli, Connexin 43 functions as a positive regulator of stem cell differentiation into definitive endoderm and pancreatic progenitors, iScience **19**, 450 (2019).

[37] J. Cervera, A. Alcaraz, and S. Mafe, Membrane potential bistability in non-excitable cells as described by inward and outward voltage-gated ion channels, J. Phys. Chem. B **11**, 12444 (2014).

[38] J. Cervera, A. Alcaraz, and S. Mafe, Bioelectrical signals and ion channels in the modeling of multicellular patterns and cancer biophysics, Sci. Rep. **6**, 20403 (2016).
[39] N. Palacios-Prado and F. F. Bukauskas, Heterotypic gap junction channels as voltage-sensitive valves for intercellular signaling, Proc. Natl. Acad. Sci. USA **106**, 14855 (2009).
[40] T. Desplantez, D. Halliday, E. Dupont, and R. Weingart, Cardiac connexins Cx43 and Cx45: formation of diverse gap junction channels with diverse electrical properties, Pflugers Arch. **448**, 363 (2004).
[41] P. Brink, Gap junction voltage dependence: A clear picture emerges, J. Gen. Physiol. **116**, 11 (2000).
[42] C. D. M. Churchill, P. Winter, J. A. Tuszynski, and M. Levin, Electroceutical design environment: An ion channel database with small molecule modulators and tissue expression information, iScience **11**, 42 (2019).
[43] S. M. Busse, P. T. McMillen, and M. Levin, Cross-limb communication during Xenopus hindlimb regenerative response: non-local bioelectric injury signals, Development **145**, 164210 (2018).
[44] O. V. Aslanidi, O. A. Mornev, O. Skyggebjerg, P. Arkhammar, O. Thastrup, M. P. Sørensen, P. L. Christiansen, K. Conradsen, and A. C. Scott, Excitation wave propagation as a possible mechanism for signal transmission in pancreatic islets of Langerhans, Biophys J. **80**, 1195 (2001).
[45] J. Cervera, S. Meseguer, and S. Mafe, MicroRNA intercellular transfer and bioelectrical regulation of model multicellular ensembles by the gap junction connectivity, J. Phys. Chem. B **121**, 7602 (2017).
[46] A. D. Lander, How cells know where they are, Science **339**, 923 (2013).
[47] C. M. Glen, M. L. Kemp, and E. O. Voit, Agent-based modeling of morphogenetic systems: Advantages and challenges, PLoS Comput. Biol. **15**, e1006577 (2019).
[48] D. E. White, M. A. Kinney, T. C. McDevitt, and M. L. Kemp, Spatial pattern dynamics of 3D stem cell loss of pluripotency via rules-based computational modeling, PLoS Comput. Biol. **9**, e1002952 (2013).
[49] V. R. Rao, M. Perez-Neut, S. Kaja, and S. Gentile, Voltage-gated ion channels in cancer cell proliferation, Cancers **7**, 849 (2015).
[50] M. Yang and W. J. Brackenbury, Membrane potential and cancer progression, Front. Physiol. **4**, 185 (2013).
[51] D. J. Blackiston, K. A. McLaughlin, and M. Levin, Bioelectric controls of cell proliferation: Ion channels, membrane voltage and the cell cycle, Cell Cycle **8**, 3527 (2009).
[52] P. G. Barghouth, M. Thiruvalluvan, and N. J. Oviedo, Bioelectrical regulation of cell cycle and the planarian model system, Biochim Biophys Acta **1848**, 2629 (2015).
[53] M. B. Bhavsar, L. Leppik, K. M. Costa Oliveira, and J. H. Barker, Role of bioelectricity during cell proliferation in different cell types, Front. Bioeng. Biotechnol. **8**, 603 (2020).
[54] B. Hille, *Ion Channels of Excitable Membranes* (Sinauer Associates, Sunderland, MA, 1992).
[55] F. Durant, J. Morokuma, C. Fields, K. Williams, D. S. Adams, and M. Levin, Long-term, stochastic editing of regenerative anatomy via targeting endogenous bioelectric gradients, Biophys. J. **112**, 2231 (2017).
[56] J. O'Brien, Design principles of electrical synaptic plasticity, Neurosci. Lett. **695**, 4 (2019).
[57] A. C. Miller and A. E. Pereda, The electrical synapse: Molecular complexities at the gap and beyond, Dev. Neurobiol. **77**, 562 (2017).
[58] D. Banerjee, Connexin's connection in breast cancer growth and progression, Int. J. Cell Biol. **2016**, 9025905 (2016).
[59] A. M. Soto and C. Sonnenschein, The tissue organization field theory of cancer: A testable replacement for the somatic mutation theory, Bioessays **33**, 332 (2011).
[60] M. Emmons-Bell, F. Durant, J. Hammelman, N. Bessonov, V. Volpert, J. Morokuma, K. Pinet, D. S. Adams, A. Pietak, D. Lobo, and M. Levin, Gap junctional blockade stochastically induces different species-specific head anatomies in genetically wild-type Girardia dorotocephala flatworms, Int. J. Mol. Sci. **16**, 27865 (2015).
[61] A. C. L. de Lichtervelde, A. ter Heijne, H. V. M. Hamelers, P.M. Biesheuvel, and J. E. Dykstra, Theory of Ion and Electron Transport Coupled with Biochemical Conversions in an Electroactive Biofilm, Phys. Rev. Appl. **12**, 014018 (2019).
[62] M. Ribeiro, A. Elghajiji, S. P. Fraser, Z. D. Burke, D. Tosh, M. B. A. Djamgoz, and P. R. F. Rocha, Human breast cancer cells demonstrate electrical excitability, Front. Neurosci. **14**, 404 (2020).